# UWS Academic Portal

## Development of measurement system and analysis method for characterization of linear variable bandpass filters

ZHou, Shun; Song, Shigeng; Cai, Sijia; Han, Daxing; Wu, Zhentao; Song, Jian; Lu, Bo; Jiang, Zhengping; Lovering, David; Liu, Weiguo; Gibson, Des

# Development of measurement system and analysis method for characterization of linear variable bandpass filters

**SHUN ZHOU,**[1] **SHIGENG SONG,**[2,3,*] **SIJIA CAI,**[2] **DAXING HAN,**[2] **ZHENTAO WU,**[2] **JIAN SONG,**[2] **BO LU,**[2] **ZHENGPING JIANG,**[2] **DAVID LOVERING,**[4] **WEIGUO LIU,**[1] **AND DES GIBSON**[2,3] (iD)

[1] *School of Opto-electronical Engineering, Xi'an Technological University, Xi'an 710021, China*
[2] *Institute of Thin Films, Sensors and Imaging, Scottish Universities Physics Alliance (SUPA), University of the West of Scotland, Paisley, PA1 2BE Scotland, UK*
[3] *AlbaSense Ltd. High Street, Paisley, PA1 2BE Scotland, UK*
[4] *Aquila Instruments Limited, Unit 9, The Maltings, Station Road, Newport, Essex CB11 3RN, United Kingdom*
*[*] shigeng.song@uws.ac.uk*

**Abstract:** An automated measurement system was developed to characterize the spatial gradient, linearity of the spatial gradient, bandwidth and transverse uniformity of a linear variable filter (LVF). To demonstrate this, the LVF fabricated in our group has been measured and analyzed. Simulations for beam spot size effects on measurements were performed for various LVF spectral peak profiles with results indicting significant averaging effect due to beam spot size and this is consistent with experiment results. Moreover, to fit the peak profile more accurately, a modified Pearson VII function was proposed and demonstrated high capability to express complex shapes of peaks mathematically. This provides a methodology for deconvoluting the original LVF peak profile from a measured averaged peak profile and has been verified using actual measured data.

## 1. Introduction

A spatially linear variable filter allows linear tuning of spectral transmission /reflection along one direction of the filter while the spectral functionality remains uniform along the direction perpendicular to gradient direction. LVFs include Short Wave Pass Filters (SWPF); Long Wave Pass filters (LWPF); Dichroic and Band Pass Filter (BPF) and can cover ultra-violet, visible and infrared wavelength ranges. Such LVF filters have a wide range of applications with a particular use in miniaturized spectrometer, multi-spectral and hyper-spectral imaging or sensing, all of which are of importance for remote imaging and sensing in environmental, agricultural and climate monitoring [1–3].

The applications of LVFs in miniaturized spectrometer attracted high attention because LVFs may dramatically reduce spectrometer size and costs while improving spectrometer performance (e.g., faster response). Another notable advantage of using LVFs for miniaturized spectrometer is that it removed need for using moving parts in traditional spectrometers due to presence of diffractive gratings. For example, A Emadi et al. developed a Fabry-Perot type of LVF for ultraviolet micro-spectrometer for potential applications for the wavelength range from 310 to 400nm in atmospheric gas sensing, pharmaceutical analysis, bimolecular identifications [4]. The authors also developed IR micro-spectrometers (wavelength range from 1400 to 2500 nm and from 3000 to 5000nm) for the potential applications in liquid identification and gas sensing [5]. B Wiesent et al. investigated LVF using static multi element detector and a scanning single

element detector for the application of oil condition monitoring for offshore wind turbines [6]. M Muhiyudin et al. also developed miniaturized infrared spectrophotometer for multi-gas sensing with low power consumption by using a LVF for the wavelength range from 2.9 um to 4.8 um with 1.5% band width referring to the central wavelength of passband [7].

The applications of LVFs in hyperspectral imaging are also attracting much attention, for example, biomedical imaging [8,9]. Hyper-Spectral Imaging (HSI) by combining spectroscopy and imaging can provide non-destructive / non-invasive analysis, this method adds spectral information onto each pixel of a 2 spatial dimensional detector array. It has been widely recognized that spectroscopy has the potential to provide "spectral signatures" for the type and grade of tissue lesions by simply measuring absorption, fluorescence, or (elastic, non-elastic) scattering spectral signals. Other applications of hyperspectral imaging are also explored, for example, S Song et al. developed a prototype for low-cost hyperspectral imaging camera in the application of agriculture. Compared to a high-end pushbroom HSI with similar specifications, this prototype camera was comparable with it in terms of performance while only costing approximately 10% of the reference system [1].

There are several approaches for producing LVFs. The simplest Fabry-Perot type of LVFs consists of a dielectric spacer with wedge thickness distribution clamped by metal layers with uniform thickness distribution on both sides as mirrors. For example, Peng Ji et al. fabricated linear variable color filters using e-beam evaporation process for a portable micro-spectrometer, where $TiO_2$ is used as the dielectric spacer and Ag is used as mirrors [10]. The advantage of this approach is that the dielectric spacer layer in the proposed filter were fabricated via glancing angle deposition without the help of any mask or moving parts. However, this structure has a disadvantage of light loss from metal layer absorption. To avoid this metal layer absorption, A Emadi developed LVF consisting of dielectric central cavity with wedge thickness distribution and two dielectric mirrors with uniform thickness distribution on both sides of cavity layer [4]. The fabrication of $SiO_2$ wedge layer involves an IC compatible reflow process where photoresist was spin coated and patterned with a special pattern design to produce a constant thickness slope after reflow. The mirrors layers are $HfO_2$ (High index) and $SiO_2$ (Low index).

To improve the performance of LVFs with high resolution and high transmittance, another approach of LVF fabrication is developed by varying all multilayer thicknesses to form a wedge shape of filters including cavities and mirrors. Considering LVF application on 2D matrix detector arrays, high linearity of wavelength spatial variation along thickness gradient direction is necessary together with good uniformity along the direction perpendicular to gradient direction (transverse uniformity). L Abel-Tiberini and F. Lemarquis, et al. specifically developed masking mechanisms and design to produce several LVFs simultaneously with a minimum of 99.8% transverse uniformity, therefore a complicated mask design is required. They also investigated the uniformity of the LVFs produced by using Dual Ion Beam Sputtering system with specifically designed mask [11–13]. Another consideration for LVF fabrication is the cost. T Moein fabricated porous polymer structures with controllable pore size and location to produce compact graded photonic bandgap structures for linear variable optical filters using holographic polymer dispersed liquid crystal materials [14]. S Song et al. also developed a cost-effective patented process for LVF fabrication using drum-based sputtering system with the aid of theoretical modelling and simulation for mask design [1,15]. The technique is not just obtaining high linearity of wavelength spatial gradient and transverse uniformity, but also enabled volume production of LVFs (around 800 LVFs per single fabrication process).

Above discussions have demonstrated that fabrications and applications of LVF were widely investigated. However, the properties and characterization of LVF still need more attention. In this work, we present the development of a novel characterization method and automated measurement system for our LVFs based on an existing spectrophotometer (Aquila nkd-8000) with updated optics for beam spot size control for light source and developed scripts for equipment

control providing automated LVF measurements. The LVF analysis methods are also proposed and presented. The LVF samples discussed in this paper were fabricated using a drum-based microwave assisted pulse magnetron sputtering. The details of fabrication can be found in our previous publication [1].

## 2. Optics and scripts of measurement equipment

The sample motion stage, light beam incident, transmission and reflection arms are shown in Fig. 1. The original incident beam is approximately collimated beam with diameter around 3 mm. An additional lens system was attached to the incident arm in order to adjust beam spot diameter from 0.5 mm to 3 mm on sample surface which can particularly useful for LVF measurements. Owing to the very wide spectral coverage of the instrument, it was not possible to make the lens system achromatic and retain adequate transmission in the ultraviolet. However, the variation of spot size with wavelength is of the order of 60μm, which has negligible effect on the interpretation of our results. The resolution bandwidth is selectable and also varies with wavelength; for these measurements it was 0.5nm in the ultraviolet, increasing to 1nm in the near infrared range. The sample stage is computer-controlled with 2.5μm resolution in both axes. The arms of the spectrophotometer are adjustable, and in this work the measurements were done at normal incidence.
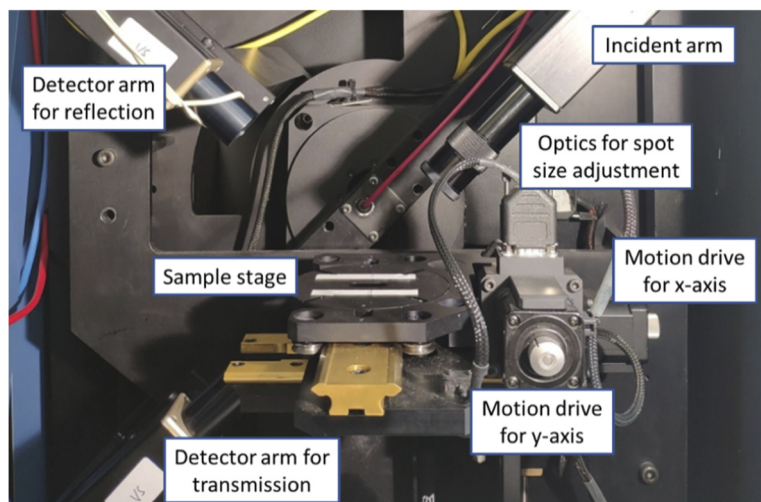


**Fig. 1.** Schematic diagram of measurement set-up including motion stage, incident beam arm and T, R detector arms.

It would be useful to have automatic scan function for LVF measurement as there is a need to collect spectral data such as transmittance (T) and reflectance (R) over the whole range of the spatial positions of the LVF sample (2D scan). For this purpose, a script was developed using the instrument's scripting language to control motion stages and collect the data. The script structure follows the steps: 1. Define reference sample position; 2. Define measurement parameters: range and step size of wavelength, incidence angles, T, R, polarization and substrate thickness; 3. Define measurement positions on sample; 4. Reference measurements for T&R; 5. Define the name for data files for series measurements; 6. Move to the first position on sample; 7. T&R measurement for sample and normalized against reference data; 8. Save measured T&R data; 9. If final measurement position, then exit after saving; otherwise loop process from step 7.

## 3.    Properties of LVFs for characterization

There are several LVFs such as SWPF, LWPF, BPF, etc. Here BPF is used as an example to discuss the properties of LVF for characterization. As shown in Fig. 2, the centre wavelength of passband of LVF varies along one direction of the filter linearly (x direction) while the spectral functionality maintains high transverse uniformity (y direction) along the direction perpendicular to wavelength gradient direction. Regarding the LVF specifications, there are optical properties that need to be defined for optical characterization in addition to geometrical size, mechanical properties of LVF, etc.
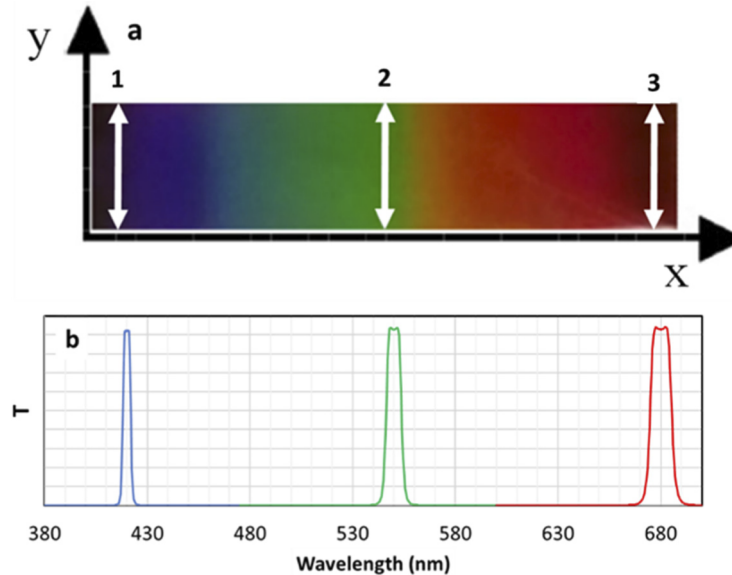


**Fig. 2.** Images of LVF sample with transmission bands as marked in respective positions.

**Spatial gradient of LVF:** wavelength span range for a certain physical length of LVF at x-direction is a critical parameter for LVF application. For example, the length of LVF needs to match the length of one-dimensional detector array for a miniaturized spectrometer development. This parameter can be defined as the special gradient of LVF which is the ratio of the wavelength span range to the effective physical length of LVF. Its unit is nm/mm.

**Linearity of LVF spatial gradient:** linear relation between center wavelength of passband and physical position on LVF provides advantage for applications. The linear equation can be obtained by fitting the measured data. There is deviation between the wavelength obtained by measurement and the one obtained using the equation. However, this error must be at an appropriate level to remain within tolerance. There is more than one way to define and parameterize this error: one method can be directly using the wavelength error e.g. $\pm\Delta\lambda$ over wavelength range from $\lambda_1$ to $\lambda_2$; another method is using the R-square based on linear regression for measured data fitting (the R-square can be obtained using linear regression function in Microsoft Excel).

**Bandwidth of Passband:** The bandwidth of passband filter directly affects measurement resolution of wavelength. The bandwidth can be defined as a half width at half maximum (HWHM). However, the HWHM is not constant over the interest wavelength range of LVF. For example, the HWHM at short wavelength side is smaller than the one at long wavelength side as shown in Fig. 1. The HWHM is proportional to the center wavelength of LVF passband when Fabry–Pérot cavity is used for design and it is based on the assumption that refractive index was kept constant over the wavelength range for LVF. Therefore, it would be useful to define the

bandwidth of LVF as the percentage of center wavelength of passband. As discussed later, the measured HWHM is different with original design HWHM due to average effect.

**Transverse uniformity:** As shown in Fig. 2, the center wavelength of passband at y-direction need to be constant. However, it may be not the case due to the difficulty of fabrication process. Transverse uniformity can be defined as the error of center wavelength over LVF covered wavelength range. But for real measurement, it needs to be considered that it is difficult to align sample at perfect x and y direction.

There are optical parameters for LVF optical characterization such as: peak intensity of passband, wavelength range, out-of-band blocking and angle tolerance range of LVF for application etc.

## 4. Simulations of beam spot size effects on measurement

The light beam spot size for most spectrometers are roughly in the millimeters range. For uniform optical thin film device, this is not a problem. However, the beam spot size needs to be considered for LVF optical analysis due to gradient thickness. The passband wavelength varies along x-direction of the LVF as shown in Fig. 1. Therefore, the measured transmission is, actually, an averaged result over the incident beam spot area. This is the beam spot size effect for LVF optical measurement. Ideally, accurate passband feature can be obtained only when the beam spot size tends to zero.

There are some assumptions being made to simplify the simulation: 1), all refractive indices of thin films for bandpass filter are constant: therefore, the HWHM of LVF can be determined as the percentage of center wavelength of passband; 2), light beam is approximately collimated, thus influence of incident angle distribution can be neglected; 3), the light is highly monochromatic; 4) simulations were done for normal incidence for comparison with experimental measurements. The beam spot in this investigation has a circular shape with a radius r.

The shape of a passband peak without average effect can be defined as $T(\lambda, \lambda_c)$ where $\lambda_c$ is the center wavelength of passband. When the beam spot has a certain size, the beam spot covers a range of x, as shown in Fig. 1, and the center wavelength of passband depends on the x value:

$$\lambda(x) = \lambda_c - x \cdot g_s \tag{1}$$

Here $g_s$ is the spatial gradient of LVF and set the center position of spot x=0. Then the measured transmission with average effect can be obtained:

$$T_{aver}(\lambda, \lambda_c) = \frac{1}{\pi r^2} \int_{-r}^{r} 2 \cdot \sqrt{r^2 - x^2} \cdot T(\lambda, \lambda_c + x \cdot g_s) dx \tag{2}$$

Starting from the simplest example: a square passband without average effect (or measured where the beam spot size intends to be zero) can be described with the following function:

$$T_{aver}(\lambda, \lambda_c) = \begin{cases} T_{\max}, if \ \lambda_c - \lambda_c \cdot p_{bw} \leq \lambda \leq \lambda_c + \lambda_c \cdot p_{bw} \\ 0, \ otherwise \end{cases} \tag{3}$$

Here $T_{\max}$ is the height of transmission peak, $\lambda_c$ is the center wavelength of passband at the center of beam spot and $p_{bw}$ is the percentage of HWHM to center wavelength. The simulation results calculated using Mathcad 15 are shown in Fig. 3 above.

Comparing to a square shape of transmission passband, a more general function is chosen for the second simulation example, the Pearson VII distribution function as shown in Eq. (4). It is convenient to use this equation for peak fitting as the HWHM and the maximum intensity ($I_{\max}$)
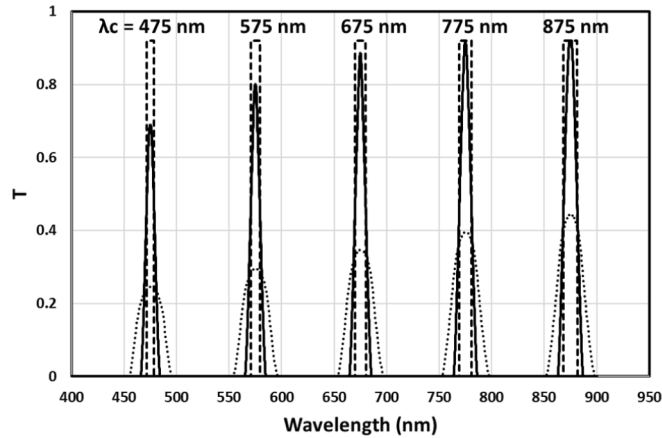
**Fig. 3.** Simulations of average effect of LVF for square original passband with $p_{bw}=0.75\%$, designed $T_{max} = 0.92$ and various center wavelengths $\lambda_c$. The spatial gradient of LVF ($g_s$) is 11.25nm/mm. For measurement beam spot radius, thick dot line: $r \rightarrow 0$; solid line: r=0.5 mm; thin dot line: r = 1.5 mm.

of the peak can be directly shown in the equation.

$$I(\lambda, \lambda_c) = \frac{I_{max}HWHM^{2m}}{[HWHW^2 + (2^{1/m} - 1) \cdot (\lambda - \lambda_c)^2]^m} \tag{4}$$

where $\lambda_c$ is the center wavelength of passband and m is the parameter to adjust the shape of peak. The shape is not sensitive to the change of m when m is higher than 10. The Pearson VII distribution function will be the same as the Cauchy–Lorentz distribution function when m=1.

Wavelength is used as variable in Eq. (4), then the peak is symmetrical to the line $\lambda = \lambda_c$ as the term $(\lambda - \lambda_c)^2$ in the function. However, the transmission band from the design using Fabry–Pérot cavities is slightly asymmetrical where the edge at short wavelength side is slightly steeper than the one at long wavelength side. It is still a good approximation to use the Pearson VII distribution function for simulation as the asymmetry is not significant.

As discussed previously, it is better to use percentage for describing the bandwidth ($P_{bw}$). Thus Eq. (4) can be expressed as:

$$I(\lambda, \lambda_c) = \frac{I_{max} \cdot (\lambda_c \cdot p_{bw})^{2m}}{[(\lambda_c \cdot p_{bw})^2 + (2^{1/m} - 1) \cdot (\lambda - \lambda_c)^2]^m} \tag{5}$$

Using Eq. (2) and Eq. (5), the simulations have been completed and is shown in Fig. 4. Further discussions on modifications to the Pearson function for peak fitting is described in the experimental data analysis section.

The above two examples show that beam spot size has a clear effect on measurement results, such as the height and width of the spectral transmission peak. The shape of peak for these examples can be described analytically using functions. However, the shape of the designed passband is quite complexed and cannot be described using a simple function. Therefore, the average effect for these complexed cases needs to be carried out numerically. The circular beam spot is divided into 31 strips along the transverse direction for the following example. The average transmission can then be obtained by summing the transmissions of strips with area weighting. The calculation for average can be simplified by considering that the shape of passband based on the design of Fabry–Pérot cavities is proportional to the center wavelength when the refractive indices of films are constant. The simulation results are shown in Fig. 5.
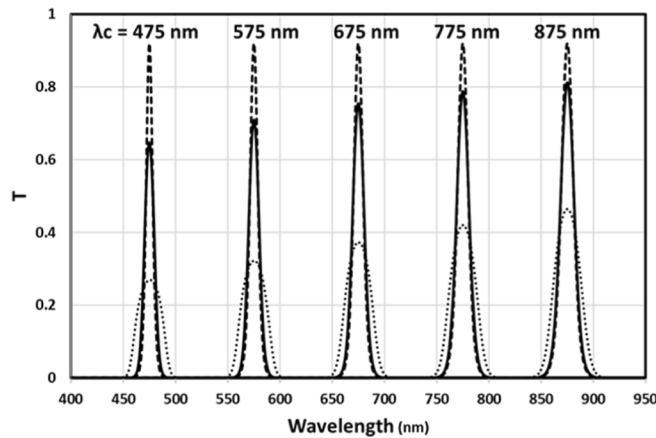
**Fig. 4.** Simulations of average effect of LVF for the original passband with Pearson function shape with $p_{bw}$=0.75%, designed $T_{max} = 0.92$, m=5 and various center wavelengths $\lambda_c$. The spatial gradient of LVF ($g_s$) is 11.25nm/mm. Thick dot line: r→ 0; solid line: r=0.5 mm; thin dot line: r = 1.5 mm for beam spot radius.



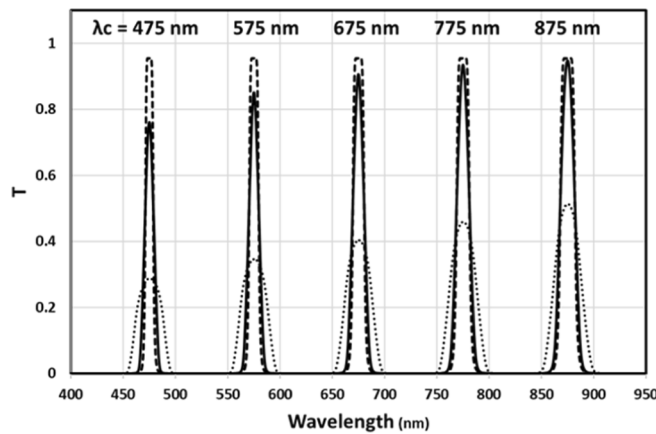**Fig. 5.** Simulations of average effect of LVF for the original passbands designed by using Fabry–Pérot cavities at various center wavelengths $\lambda_c$ with $p_{bw}$=0.835%. The refractive indices for design are 2.3113, 1.4558 and 1.5152 for high index, low index and substrate index respectively. The spatial gradient of LVF ($g_s$) is 11.25nm/mm. Thick dot line: r→ 0; solid line: r=0.5 mm; thin dot line: r = 1.5 mm.

The simulation results show that beam spot size has clear influence on average effect. Another interesting result is that the height of averaged peak at short wavelength side is lower than the one at long wavelength side even though the heights of original peaks are exactly same. Further simulations also indicate that the spatial gradient of LVF ($g_s$) and the bandwidth of passband also have high influence on average effect from beam spot size.

The beam spot size effect is not just important for LVF characterization, but also important for applications. LVF specifications needs to be considered for deciding a correct size of detector and light source beam size for spectrometer development.

## 5. Measurement results and analysis

### 5.1. Measurements using small beam spot size

LVF samples used for characterization were produced using a microwave assisted pulse magnetron sputtering process, see Ref. 1. The design of the LVF is based on Fabry–Pérot structure with 3 cavities using $Nb_2O_5$ as high index material, $SiO_2$ as low index material and microslide glass as substrate.

LVF characterization starts from a small beam spot size r = 0.4 mm because it would have less average effect on measurement according to previous simulations. Data fitting using a known function is helpful for finding accurate peak position and bandwidth. Pearson VII function and Gaussian function were both tried. However, the fitting results were not satisfactory. An example of using Pearson VII function is shown in Fig. 6. The issue is the top of the peak, which is "too sharp" and it is impossible to adjust the function to fit the shape of the peak using the current form of the function. By observing the function, it can be deduced that it would give more capability to adjust the profile of peak if the power 2 is replaced by a variable n, see Eq. (6).

$$T(\lambda, \lambda_c) = \frac{I_{max} \cdot (\lambda_c \cdot p_{bw})^{n \cdot m}}{[(\lambda_c \cdot p_{bw})^n + (2^{1/m} - 1) \cdot (\lambda - \lambda_c)^n]^m} \tag{6}$$

As such Eq. (6) maintains the previous advantages: directly defining the height of peak ($I_{max}$) and the percentage of HWHM. This is very convenient for spectrum analysis.
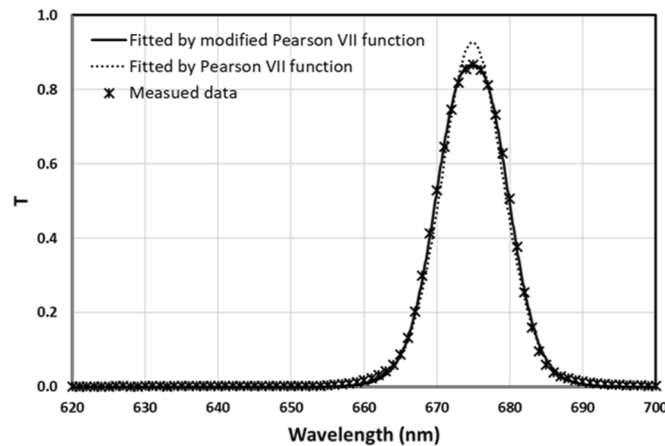


**Fig. 6.** Comparison of fitting curve to data using Pearson VII function and the modified Pearson VII function, indicating much improved fit using modified Pearson VII function.

The results shown in Fig. 6 demonstrate fitting performance is significantly improved through the use of Eq. (6) compared with Eq. (5).

All measurement data were fitted to determine the optical specification of the LVF sample, such as the center wavelength of passbands, the height of transmission band, bandwidth and spatial gradient, linearity, transverse uniformity, etc. Figure 7 shows that the fitting results agree with the peak profiles of the measurements very well over the designed physical range of 40 mm. The peak heights at left side of the figure are lower than the height of peaks in the middle of the figure, this is due to peak average effect and agrees with the simulation results. However, it is noticed that the peak heights at right side of the figure is also lower compared to middle peaks. The possible reason for this, is the dispersion of lenses used for beam focus as the beam spot size is much bigger at the near infrared range as the refractive index of lens material is lower.

The center wavelength of passband vs the physical position at x-direction on LVF is obtained from fitting results and is shown in Fig. 8. The spatial gradient $s_g$ is obtained as 10.832 nm/mm
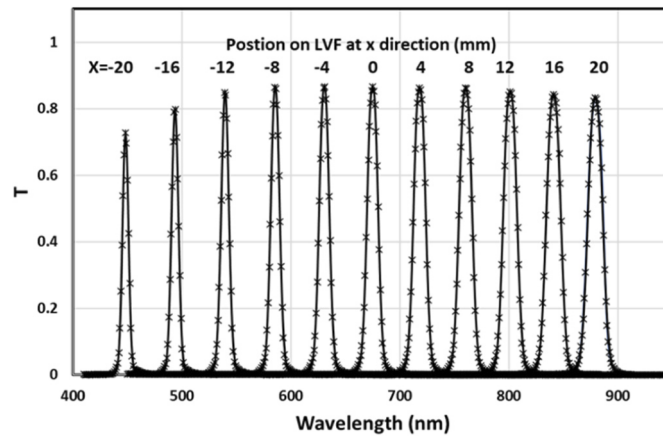
**Fig. 7.** The transmission bands over LVF sample for 40 mm range at various positions. Beam spot size r = 0.4 mm. Dots: measurements; Solid lines: fitting results using Eq. (6).

using linear regression. The error ($R^2$) is 0.9991. Refer to the linear equation, the deviation $\Delta\lambda/\lambda$ is +/- 1% for the wavelength range from 450 nm to 900 nm. Figure 8 also shows the trend of HWHM is decreasing while center wavelength of passband is decreasing because of the dispersion of refractive indices of thin film materials used in the multi-layer stack. At the center position of LVF, the center wavelength of passband is 674.9 nm, the percentage of HWHM to the center wavelength is 0.83% which is 11.2 nm for FWHM. Note, dispersion affects are neglected during a single peak fitting as the wavelength range is small.
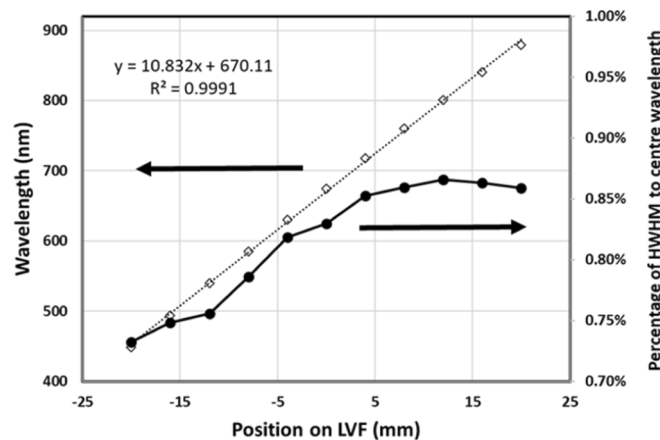


**Fig. 8.** Centre wavelengths and percentage bandwidth of passbands plotted against physical position on LVF at x-direction, measured using r = 0.4 mm beam spot size; the graph indicates high linearity of central wavelengths to position.

The measurement system developed in our group for LVF analysis has the capability to scan sample at x and y direction, this provides an ability for transverse uniformity analysis. The measurements were done using beam spot with radius r = 0.4 mm. The insert in Fig. 9(a) shows the whole peak profile. Main figure of Fig. 9(a) shows the discrepancy from point to point by zooming to smaller scales to focus on the top of the peaks.

The center wavelengths of peaks were determined by data fitting shown in Fig. 9(b). The error from the trend line for all measurements falls within +/- 0.05 nm range, which shows that the
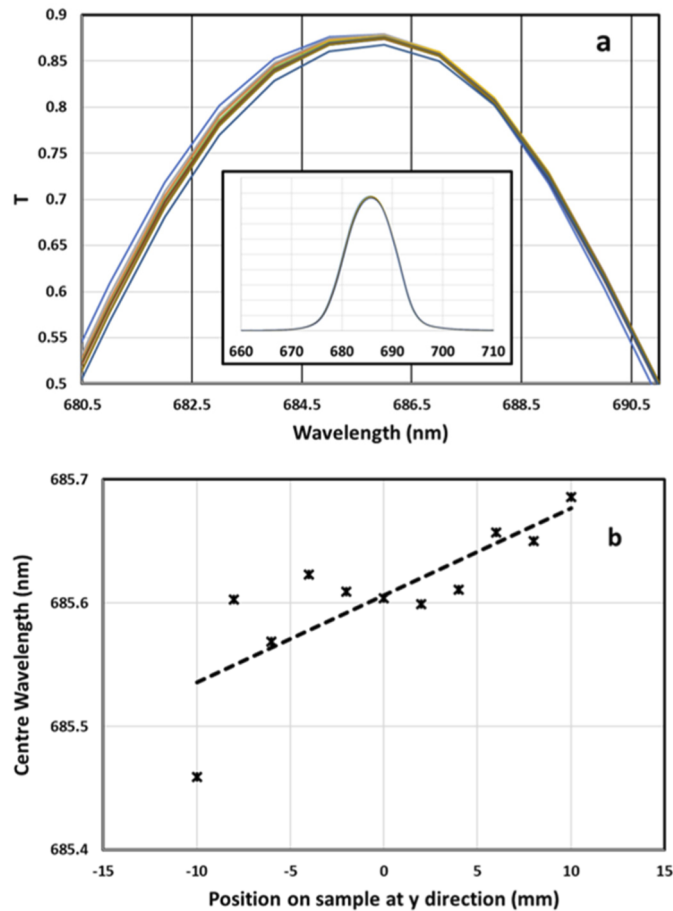
**Fig. 9.** a) The measurements at y-direction over length of 20 mm with interval 2 mm for transverse uniformity analysis, with zoom-in image of top of peak; b) Central wavelength against position on sample at y-direction with trendline.

LVF developed using our deposition system has extremely high transverse uniformity. The trend line also suggested that the sample placed on motion stage may not be perfectly aligned with the y direction.

### 5.2.   *Data analysis with the considerations of average effect*

In section 3, average effect was simulated starting from a known peak profile. It would be useful if we can reverse the process: that is start from an averaged peak profile, for example, measured LVF transmission passband with a certain beam spot size, then obtain the original peak profile mathematically. The methodology is: 1, set a function for a possible profile before averaging using Eq. (6); 2, set initial guesses for parameters; 3, using Eq. (1) and Eq. (2) and integrate over circular beam spot; 4, calculate the error comparing with the known averaged peak profile; 5, using Levenberg-Marquardt nonlinear regression to find a new set of parameters; 6, iterate error calculation and nonlinear regression until satisfied parameters are obtained.

To verify the feasibility of this methodology, the averaged peak profile in Fig. 5, which was calculated numerically at r=1.5 mm beam spot, is used to work out a theoretical passband profile designed using 3 Fabry–Pérot cavities. The impressive results are shown in Fig. 10. The

calculation starts from the data labelled by crosses in Fig. 10, then followed above methodology to obtain the design profile (white dash line). It shows excellent agreement with the original design profile (thick black line). This also demonstrates that the modified Pearson VII function, Eq. (6), has very high flexibility to adjust for the shape of peak. It can be Cauchy-Lorentz shape, peak with flat top or even a square shaped peak.
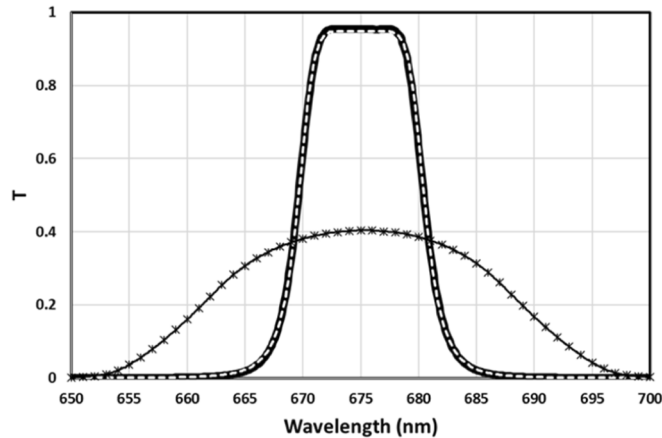


**Fig. 10.** The verification of the feasibility for a reversed calculation process: work out original passband profile from a simulated measurement profile with average effect using a beam spot with 1.5 mm radius for a LVF with spatial gradient of 11.25 nm/mm. Cross: simulated measurement data; dashed white line: a possible original peak obtained by fitting the cross dots; thick black line: original design profile. The parameters for the modified Pearson function are: $I_{max} = 0.95$, $\lambda_c = 675$ nm, $P_{bw}=0.814\%$, m=0.656, n=8.38.

The average effect of LVF measurement was demonstrated by simulation as well as confirmed by experimental measurement. The LVF sample analyzed in Section 5.1 using r=0.4 mm beam spot was also measured at r = 1.5 mm as shown in Fig. 11. This has a further demonstration for average effect due to beam spot size. The widths of peaks are broadened, and the heights of peaks decreases when the center wavelengths of passbands decrease.
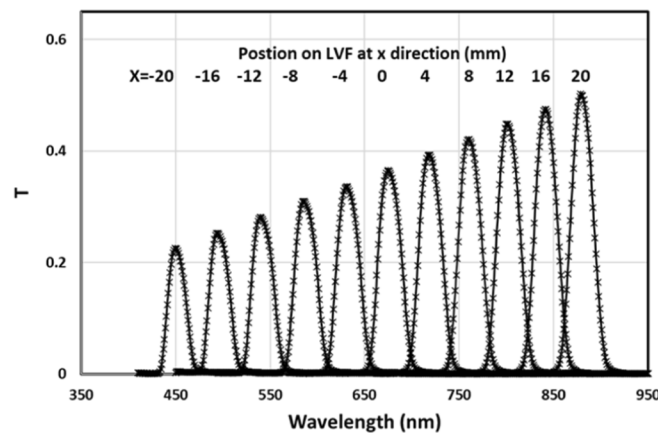


**Fig. 11.** Measured transmissions on LVF sample over various position using a beam spot with radius 1.5 mm.

Continuing the method for extracting original passband profile based on simulation results, we now use same method to verify the possibility to extract original passband profile based real measured data of an actual LVF sample. The measured data at the center position of the LVF are used for calculations. The calculation results are shown in Fig. 12. The extracted shapes of the peaks are highly similar for both beam spot diameters. However, it is found that the extracted profiles from measured data using beam spots with 0.4 mm and 1.5 mm diameter have very different peak height even though they were obtained at the same spot on the sample. One possible reason for this issue could be the uniformity of light intensity over spot area is not high enough; another reason could be that the reading for spot size is not accurate. Small error of spot size may cause a big change for peak profile extraction.
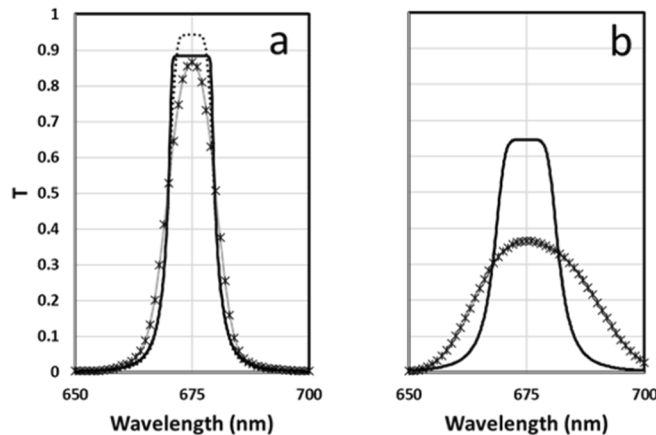


**Fig. 12.** Extractions of possible original passband profile based measured transmission passband of LVF using modified Pearson VII function. In a, cross: measured data using beam r = 0.4 mm; black solid line: extracted profile using r = 0.4 mm; dotted line: extracted profile using r = 0.45 mm; In b, cross: measured data using beam r = 1.5 mm; black solid line: extracted profile using r = 1.5 mm.

For example, the peak profile with dotted line in Fig. 12(a) extracted using a diameter of 0.45 mm is quite different with the one with solid black line in Fig. 12(a) extracted using a diameter of 0.4 mm. A further study is needed by considering the uniformity of light intensity of the incident beam spot, accurate determination of beam spot size, dispersion of incident beam optics as well as considering the monochromaticity of incident beam.

## 6. Conclusions

An automated system has been developed based on an existing spectrophotometer with updated optics for light source beam spot size control, motion stage for 2D scan on sample surface with accuracy of 2.5um and C-like scripts for equipment control of sample locating and spectrum collection, which are particularly useful for LVF measurements. This paper discussed the parameters for LVF characterization, such as spatial gradient of LVF, linearity of LVF spatial gradient, bandwidth of passband and transverse uniformity. As an example of using this characterization system, the LVF fabricated in our group has been measured and analyzed. The results obtained for the specifications of this LVF are: spatial gradient is 10.832 nm/mm with linearity of $R^2 = 0.9991$, effective wavelength range of LVF is 450 nm to 900 nm, the center wavelength of passband at middle position of LVF is 674.9 nm, the percentage of HWHM to the center wavelength is 0.83% which is 11.2 nm for FWHM at the middle potion of LVF. The results demonstrated very high transverse uniformity within +/- 0.05 nm range for 20 mm range.

Based on described assumptions for simplification, simulations for beam spot size effects for measurement were done for various peak profile such as square shape, Pearson VII function and designed complex peak profile using Fabry–Pérot cavities. These simulation results indicted significant beam spot size averaging effect. The average effect of beam spot size was also confirmed by experimental measurements using measurement done with beam spot diameters of 0.4 mm and 1.5 mm.

In order to fit the peak profile more accurately, particularly for the peak profile generated by bandpass filter designed using Fabry–Pérot cavities, this paper proposed a modified Pearson VII function. The modified Pearson VII function has very high flexibility to adjust for the shape of peak. It has the capability of mathematically expressing Cauchy-Lorentz shape, peaks with flat top or even square-shaped peaks. The modified Pearson VII function can also be useful for other spectral analysis with complex peak shapes.

A mathematical methodology was also proposed in this paper for reverse extracting the original spectral transmission peak profile from a known averaged peak profile. The first example discussed in the paper, i.e., the peak with beam spot (diameter is 1.5 mm) average effect which is calculated numerically from a theoretical passband profile designed using 3 Fabry–Pérot cavities, verified the feasibility of this methodology. The extracted peak has excellent agreement with the original design spectral transmission profile. The methodology was also verified using real measured data of an actual LVF sample. It also demonstrated that it is possible to extract original peak profile from measured peak profile which has unavoidable average effect due to beam spot size. However, there are further issues for future investigations to improve calculation, such as: uniformity of light intensity of incident beam spot, accurate determination of beam spot size, dispersion of incident beam optics as well as considering the monochromaticity of incident beam.

**Disclosures.** The authors declare no conflicts of interest.

**Data availability.** Data underlying the results presented in this paper are not publicly available at this time but may be obtained from the authors upon reasonable request.

## References

1. S. Song, D. Gibson, S. Ahmadzadeh, H. Chu, B. Warden, R. Overend, F. Macfarlane, P. Murray, S. Marshall, M. Aitkenhead, D. Bienkowski, and R. Allison, "Low-cost hyper-spectral imaging system using a linear variable bandpass filter for agritech applications," Appl. Opt. **59**(5), A167–175 (2020).
2. X. Yu, Q. Lu, H. Gao, and H. Ding, "Development of a handheld spectrometer based on a linear variable filter and a complementary metal-oxide-semiconductor detector for measuring the internal quality of fruit," J. Near Infrared Spectrosc. **24**(1), 69–76 (2016).
3. R. A. Crocombe, "Portable Spectroscopy," Appl. Spectrosc. **72**(12), 1701–1751 (2018).
4. A. Emadi, H. Wu, G. Graaf, P. Enoksson, J. Correia, and R. Wolffenbuttel, "Linear Variable Optical Filter-based Ultraviolet Microspectrometer," Appl. Opt. **51**(19), 4308–4315 (2012).
5. A. Emadi, H. Wu, G. de Graaf, and R.F. Wolffenbuttel, "IR Microspectrometers based on Linear-Variable Optical Filters," Procedia Eng. **25**, 1401–1404 (2011).
6. B. R. Wiesent, D. G. Dorigo, O. Simsek, and A. W. Koch, "Liner Variable Filter Based Oil Condition Monitoring System for Offshore Windturbines," *Proc. of SPIE*, 8105, 81050D (2011).
7. M. Muhiyudin, D. Hutson, D. Gibson, E. Waddell, S. Song, and S. Ahmadzadeh, "Miniaturised Infrared Spectrophotometer for Low Power Consumption Multi-Gas Sensing," Sensors **20**(14), 3843–3862 (2020).
8. C. Balas, C. Pappas, and G. Epitropou, "Multi/Hyper-Spectral Imaging," in: D. Boas, C. Pitris, and N. Ramanujam (Eds.), *Handbook of Biomedical Optics* CRC Press, 2011, pp. 131–164.
9. H. Fabricius and O. Pust, "Linear Variable Filters for Biomedical and Hyperspectral Imaging Applications," *Conference Paper of Biomedical Optics*, Miami USA, April 2014.
10. P. Ji, C. Park, S. Gao, S. Lee, and D. Choi, "Angle-tolerant linear variable color filter based on a tapered etalon," Opt. Express **25**(3), 2153–2161 (2017).

11. L. Abel-Tiberini, F. Lemarquis, and M. Lequime, "Masking Mechanisms Applied to Thin Film Coatings for the Manufacturing of Linear Variable Filters for Two-dimensional Array Detectors," Appl. Opt. **47**(30), 5706–5714 (2008).
12. L. Abel-Tiberini, F. Lemarquis, G. Marchand, L. Roussel, G. Albran, and M. Lequime, "Manufacturing of linear Variable Filters with Straight Is0-thickness Lines," Proc. SPIE **5963**, 59630B (2005).
13. F. Lemarquis, L. Abel-Tiberini, C. Koc, and M. Lequime, "400-1000 nm All Dielectric Linear Variable Filters for Ultra Compact Spectrometer," *International Conference on Space Optics*, Rhodes Greece, Oct 2010.
14. T. Moein, D. Ji, X. Zeng, K. Liu, Q. Gan, and A. Cartwright, "Holographic Photopolymer Linear Variable Filter with Enhanced Blue Reflection," ACS Appl. Mater. Interfaces **6**(5), 3081–3087 (2014).
15. S. Song, D. Gibson, and D. Hutson, "Apparatus and Methods for Depositing Variable Interference Filters," patent application number GB1702478.7, priority date 15th February 2017, https://worldwide.espacenet.com/searchResults?compact=false&DB=EPODOC&PN=WO2018150173